Novella Rosa, R.; Gómez-Soriano, J.; Martínez-Hernándiz, PJ.; Libert, C.; Rampanarivo, F. (2021). Improving the performance of the passive pre-chamber ignition concept for spark-ignition engines fueled with natural gas. Fuel. 290:1-11. https://doi.org/10.1016/j.fuel.2020.119971

Improving the performance of the passive pre-chamber ignition concept for spark-ignition engines fueled with natural gas

R. Novella[a], J. Gomez-Soriano[a,*], P. J. Martinez-Hernandiz[a], C. Libert[b], F. Rampanarivo[b]

[a]*CMT – Motores Térmicos, Universitat Politècnica de València, Camino de Vera, 46022 Valencia, Spain*
[b]*DEA-IRP Groupe Renault, 1 avenue du Golf. 78084, Guyancourt, France*

Abstract

Passive pre-chamber ignition concept has been proven to be an excellent strategy to increase the ignition energy and enhance the combustion velocity even when spark-ignition engines are operating in diluted conditions. Other benefits of this system are the increased combustion stability and combustion efficiency, reducing hydrocarbons and carbon monoxide emissions. However, these advantages are limited at some operation conditions such as low engine load or diluted conditions since both the energy available in the pre-chamber and the scavenge of combustion products are compromised. In this framework, numerical studies using two different computational tools, based on one-dimensional modeling, are utilized to gain knowledge about the governing parameters and to improve the design of a pre-chamber when the engine operates at these restrictive conditions. In particular, the impact of the pre-chamber volume, the total cross sectional area of the holes and tangential angle of the nozzles has been numerically evaluated. Different pre-chamber designs were proposed and experimentally tested in a single-cylinder, high compression ratio turbocharged spark-ignition engine fueled with compressed natural gas and operating on Miller cycle. Results give valuable insight into the key aspects of the internal geometry and some relevant design paths to follow for a suitable pre-chamber definition.

Keywords: *Spark-Ignition Engine, Pre-chamber Ignition, Miller cycle, EGR, Efficiency, CNG*

*Corresponding author.
Tel.: +34 96 387 98 13, fax: +34 96 387 76 59
email: jogoso1@mot.upv.es

1. Introduction

Nowadays, the global levels of greenhouse gas emissions (GHG) are higher than even before. Some authors like Davis et al. [1] or Malik et al. [2] warned about the increase of the carbon dioxide (CO_2) emission, its contribution to the climate change [3] and the threat that it supposes [4]. Road transport, being one of the main contributors, forced automotive companies to increase their efforts in reducing CO_2 emissions. Since this component is an intrinsic product of hydrocarbons combustion, increasing the engine thermal efficiency helps to reduce the carbon footprint of the transportation fleet. In addition to this strategy, the use of compressed natural gas (CNG) as fuel is being evaluated due to its low carbon content (CH_4) and subsequent benefits in CO_2 emission.

In this framework, increasing efficiency at part-load conditions in spark-ignition (SI) engines is one of the most challenging ways to positively contribute to this global issue. While this strategy simplifies the engine control, the increased pumping loses strongly compromise the overall engine efficiency [5].

In the past, multiple SI engine configurations and combustion strategies have been evaluated for increasing the engine thermal efficiency. For instance, one strategy to increase the thermal efficiency at part-loads is a combination of downsizing and turbocharging [6]. Downsizing consists in reducing the engine displacement, relocating the operation point to a more efficient region in the engine map, while the global performance is kept or even increased by the improved boost conditions [7].

This combination of strategies is also compatible with exhaust gases dilution (EGR) [8]. In EGR-diluted combustions, the fuel consumption is reduced due to the lower heat losses through the walls [9], the lower pumping losses [10] and the increase in the specific heat ratio [11]. However, the main drawback of this strategy is the higher cycle-to-cycle variability (CCV) that can be reduced by increasing the ignition energy deposition [12, 13, 14]. Among a new set of technologies that are able to increase the ignition energy and reduce combustion dispersion, Turbulent Jet Ignition (TJI) [15] has been proved to be an attractive solution.

This ignition concept has been widely studied by several authors, showing clear advantages in terms of thermal efficiency that suggest a possible implementation to production engines. Attard et al. investigated the main effects of this ignition concept [16, 17, 18, 19]. Visualizations of the flame development were shown by Gentz et al. [20, 21]. Biswas et al. [22, 23, 24], Shah et al. [25] and Thelen et al. [26] studied the effects of pre-chamber (PC) volume and orifice diameter on the performance of combustion. Allison et al. [27] investigated how affects the pre-chamber efficiency to the jet dynamics, while Bunce et al. [28] studied the role of pre-chamber geometry on the jet physics. Mastorakos et al. [29] focused on the fundamentals of jet ignition, demonstrating that this ignition concept could be an interesting solution for different applications such as heavy-duty [30] and stationary engines [31, 32].

Using a passive pre-chamber ignition system, the authors observed relevant efficiency gains when operating at high load conditions with high knock restrictions [33]. Since there is no additional fuel supply inside a passive pre-chamber, the energy available for the main chamber ignition cannot be directly controlled by the fuel injection [34, 35]. In addition, the large amount of combustion products remained inside the pre-chamber after the scavenge aggravate this situation. This results in a poor combustion process that compromises the performance of the hot jets. At low engine loads, the lack of fuel mass inside the pre-chamber becomes a serious constraint that affects the overall performance of the engine, since the ejection process is extremely compromised [36].

In order to fix these issues, other authors [36] analyzed the effect of the internal geometry of the pre-chamber on combustion. For instance, the fuel mass at the start of PC combustion could be increased by modifying the pre-chamber volume, thus raising the energy available to be transferred to the hot jets. The impact of the nozzles orientation has been also evaluated by numerical simulations in [37]. This parameter controls the swirling flow movement inside the pre-chamber, conditioning its scavenge and the combustion stability. All these modifications must be compatible with high levels of external EGR operating though the whole operating load range.

The present paper frames in the context of increasing thermal efficiency, to indirectly reduce CO_2 emission, of the next generation of SI engines using a passive pre-chamber ignition system fueled by CNG. The main target of this investigation is therefore focused on identifying relationships between the pre-chamber design and its impact on the engine efficiency. For this purpose, a new numerical methodology based on one-dimensional modeling is proposed and validated using engine experiments performed in a test bench. Since the relevance of the internal pre-chamber geometry has not been extensively investigated in the literature, this work will contribute to understand in detail the impact of the new proposed designs and to optimize this combustion concept in its broadest sense.

2. Tools and methodology

2.1. Experimental tools

An experimental campaign was conducted in a turbocharged SI engine to calibrate the numerical models and to validate the numerical methodology. A baseline pre-chamber geometry, designed for operating with gasoline fuel [38], was firstly used as reference. Geometric details of the reference design are shown in Table 1.

Table 1: *Main specifications of the baseline pre-chamber.*

	Pre-chamber 1 (PC1)
Volume [mm^3]	600
Hole diameter [mm]	0.7
Hole area [mm^2]	2.3
Number of holes [-]	6
Hole tangential angle [degrees]	7.5

Using CNG fuel, a series of tests were carried out at part-load conditions to compare the performance of each pre-chamber definition. The first operating point (OP1) combined low engine speed (1350 rpm) and low engine load (2.8 bar IMEP). The second point (OP2) mixed medium-to-high engine speed (4500 rpm) and medium-to-high engine load (12.8 bar IMEP). In both operating conditions, the baseline pre-chamber and the proposed designs were contrasted against the conventional spark ignition system.

In addition, two parametric studies were performed to compare the performance of the new pre-chamber definitions. The impact of the spark timing was analyzed by advancing or delaying it 2-cad steps from the maximum brake torque (MBT) point. And, the effect of EGR dilution was studied from zero to the maximum dilution limit in steps of 5%. In both cases, tests were performed until the combustion stability was extremely compromised or the thermo-mechanical limits of the engine were reached. These activities are summarized in Table 2 which shows the maximum EGR dilution ratio achieved and the limit values of spark timings (ST) for each concept and/or pre-chamber definition.

For safety reasons, the spark timing sweep of PC1c has only three tested points since a critical cycle-to-cycle variability was observed in the whole operating range.

Table 2: *Operating settings for the experimental campaign.*

		OP1	OP2
Engine speed [rpm]		1350	4500
IMEP [bar]		2.8	12.8
SI	ST [cad]	-32 : 4 : -8	MBT
	EGR [%]	0	0 : 5 : 23
PC1	ST [cad]	-30 : 2 : -18	MBT
	EGR [%]	0	0 : 5 : 13
PC2	ST [cad]	-32 : 2 : -16	MBT
	EGR [%]	0	0 : 5 : 15
PC1b	ST [cad]	-30 : 2 : -18	MBT
	EGR [%]	0	0 : 5 : 9
PC1c	ST [cad]	-42, -14, -8	MBT
	EGR [%]	0	0 : 5 : 10

To obtain the target gross IMEP in the engine, the spark timing was swept operating with a conventional spark ignition system until reaching the MBT conditions, and then, the injected fuel mass was adjusted keeping stoichiometric conditions without EGR dilution. When this quantity of fuel was obtained, it was kept constant for all tests, including both pre-chamber and conventional SI, at the same engine speed and load conditions.

2.1.1. Engine architecture

The engine is a single-cylinder turbocharged spark ignition engine that will be found in the market in a near future in its multi-cylinder version. The main specifications of the engine can be found in Table 3. This base of the engine architecture is the same used in a previous author's work [33]. The cylinder head has four valves with double-overhead camshafts for improving the cylinder scavenging and filling. The Gasoline Direct Injection (GDI) fuel supply system was replaced by a Port Fuel Injection (PFI) system, assembled at the intake manifold to assure the homogeneity of the mixture. The valve overlap was removed to minimize short-circuit losses. The engine operates under Miller cycle in order to reduce the pumping losses. The compression ratio has been increased up to 15.4 to take advantage of the Miller functioning cycle.

Table 3: *Main specifications of the engine.*

Engine	4-stroke SI
Number of cylinders [-]	1
Displacement [cm^3]	404
Bore – Stroke [mm]	80.0 – 80.5
Compression ratio (geometric) [-]	15.4:1
Valvetrain [-]	DOHC
Number of valves/cylinder [-]	2 intake and 2 exhaust
Fuel injection system [-]	PFI (P_{max} = 6 bar)

Regarding the integration of the TJI system, the conventional spark plug and the pre-chamber body share the same housing in the cylinder head in order to facilitate the exchange between conventional and turbulent jet ignition. In Fig. 1 a sketch of the cylinder and ports is presented.

2.1.2. Test cell facility

The engine was assembled in a fully instrumented test cell as in the sketch of Fig. 2. To provide the compressed air necessary to simulate boost conditions an external compressor is employed. The exhaust backpressure is controlled by means of a throttle valve located in the exhaust line after the exhaust settling. The arbitrary levels of cooled EGR are provided by a low pressure EGR system assembled in the experimental facility. This system is able to provide the desired EGR level even when operating at high intake boost pressure.

Air-to-fuel ratio inside the main chamber was measured by a lambda sensor placed at the exhaust, and also by the exhaust analyzer HORIBA MEXA 7100 DEGR. This device also measures the EGR rate. While the average air-to-fuel ratio was calculated by dividing the fresh air mass flow rate by the injected fuel mass flow rate, removing the portion of air in the EGR. Some piezo-resistive sensors were employed to measure the instantaneous intake and exhaust pressure, while the in-cylinder pressure was measured with a piezoelectric sensor. These high frequency signals were sampled with a resolution of 0.2 cad.

Oil and water temperatures and pressures were controlled and monitored during all experimental campaign by an AVL 577 conditioner totally independent from the engine. The fuel consumption of the engine was monitored with a BRONKHORST F-113AC-M50-AAD-44-V flowmeter. Full details about this facility are provided in [33].

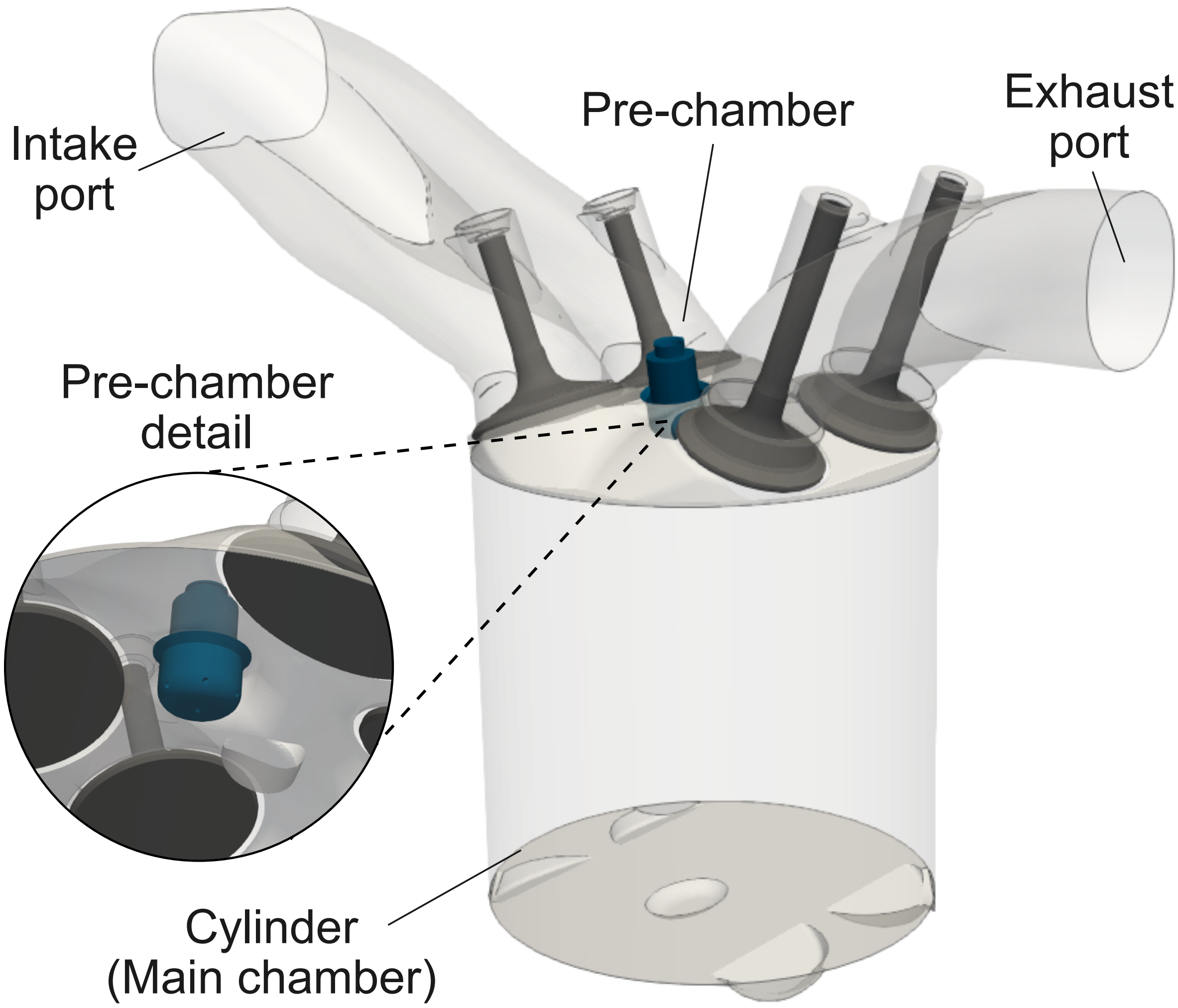

Figure 1: *Sketch of the engine design including the passive pre-chamber spatial positioning in the cylinder head.*

Tests were carried out using a calibrated compressed gas natural (CNG) fuel with a Research Octane Number of 120 (RON120). The characteristics of the fuel are given in Table. 4.

The most relevant global parameters related to the combustion process, such as the indicated gross mean effective pressure (IMEP), start of combustion (SoC), combustion phasing (CA50), combustion duration (CA10-90), maximum cylinder pressure, pressure gradient, combustion stability, heat release rate (HRR) and cylinder mean gas temperature were calculated from the cylinder pressure signal by an in-house 0D combustion diagnostics software [39, 40].

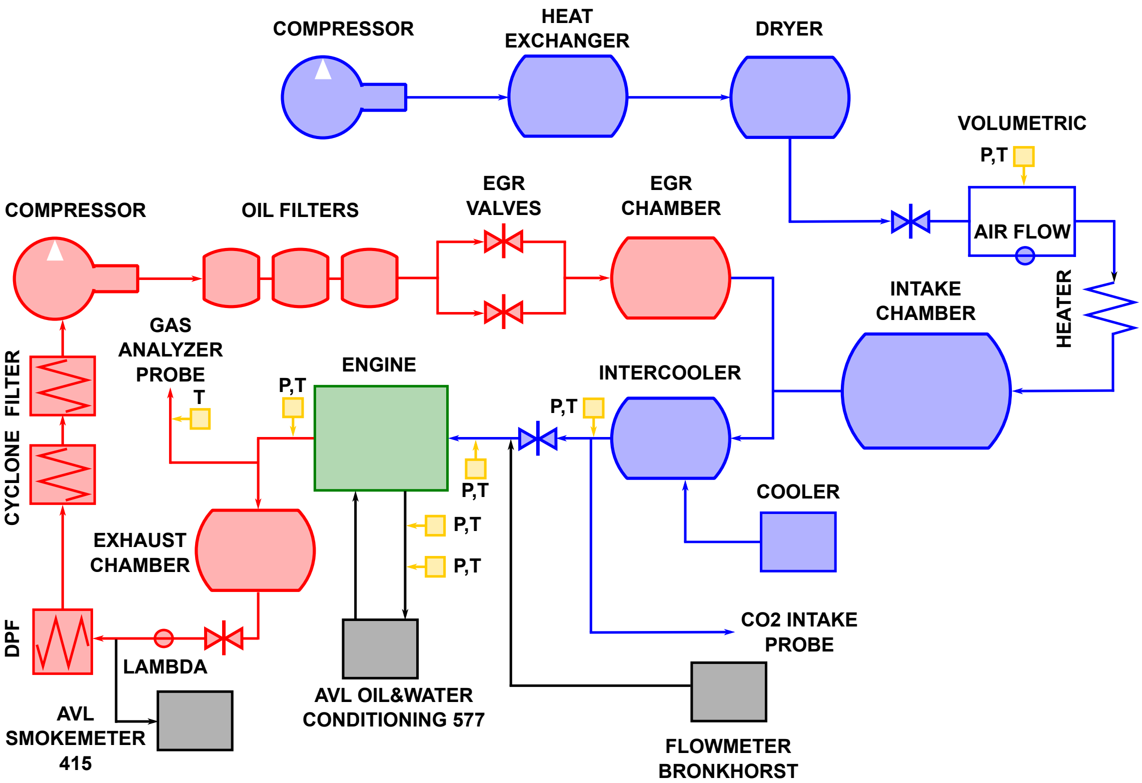

Figure 2: *Layout of the engine test cell.*

Table 4: Main specifications of the fuel.

Type	**CNG RON120**
H/C ratio [mol/mol]	3.84 mol/mol
O/C ratio [mol/mol]	0.0 mol/mol
A/F_{st} [-]	16.72
Lower Heating Value (LHV) [MJ/kg]	48.931
Density (15°C) [kg/m^3]	5
Reduced formula ($C_xH_yO_z$)	1.077 (x) - 4.137 (y) - 0.0 (z)

2.2. Modeling tools

The main target of the modeling activities was to design a passive pre-chamber suitable for operating at a wide range of conditions. Using a combination of 1D wave action and 1D jet models, to minimize the computational costs, the jet characteristics are studied and optimized by modifying some relevant parameters of the internal pre-chamber design: pre-chamber volume and total holes area.

The operating points described in the previous section were specifically selected to deal with the most extreme conditions observed in the bench. Low load/speed conditions (OP1) seem to be the main constraint of the concept since the small amount of fuel inside the pre-chamber not only reduces the available energy to ignite the main chamber mixture but also compromises a suitable temperature in the exhaust tailpipe to activate the three-way catalyst. On the other hand, the pre-chamber scavenging and filling are extremely compromised at high engine speeds (OP2).

During a first stage, numerical simulations were performed to evaluate the impact of the geometrical parameters of the pre-chamber (volume and hole total area) on the hot jets performance. In this sense, a 1D wave action model of the complete test bench facility was used to estimate the characteristics of the flow at the holes outlet. Then, with these data, a 1D jet model was utilized to compute the hot jet features inside the main combustion chamber. The optimization target is based on the principle that improved jet features (e.g. high penetration) results in an enhanced combustion process due to a larger initial surface of the flame.

After the models validation, a design of experiments (DOE) was outlined to explore different geometrical configurations and combustion profiles in the pre-chamber. The matrix of simulations is presented in Table 5. Two different set of simulations were carried out in order to clarify the effect of the pre-chamber geometry and the combustion law (through the start of combustion and the combustion duration) on the jet features. In the first set, the volume is increased from 400 to 1000 mm^3 in steps of 50 mm^3, while the holes diameter, and thus, the total holes area is increased from 0.4 to 1.6 mm in steps of 0.1 mm. In this study, the parameters of combustion within the pre-chamber were kept constant, with a start of pre-chamber combustion (SoC_{PC}) of -16 degrees ATDC and a combustion duration of 12 cad. Regarding the second set of calculations, the start of combustion is increased from -20 to -10 degrees ATDC in steps of 1 degree, while the combustion duration is increased from 8 to 20 degrees in steps of 1 degree. Here, the pre-chamber volume and holes diameter were kept constant at 600 mm^3 and 0.7 mm, respectively.

Table 5: *Summary of the simulations performed.*

		Min. value	Max. value	# levels
DOE 1	Volume [mm^3]	400	1000	13
	Hole diameter [mm]	0.4	1.6	13
	SoC_{PC} [cad ATDC]	-16	-16	1
	Comb. duration [cad]	12	12	1
DOE 2	Volume [mm^3]	600	600	1
	Hole diameter [mm]	0.7	0.7	1
	SoC_{PC} [cad ATDC]	-20	-10	11
	Comb. duration [cad]	8	20	13

2.2.1. 1D wave action model

The complete test facility was modeled using a 1D wave action software which includes both the experimental facility and the single-cylinder engine. This model was used in the author's previous work [38] with few changes in the configuration to speed up the calculation time. In this way, the intake and the exhaust lines from the original model were removed and only the pre and main chambers were kept for the calculation of the jet momentum, mass flow rate through the orifices and fuel mass at start of combustion.

This model was calibrated using both conditions described above (OP1 and OP2). Results of this procedure are presented in Fig. 3 in which the pressure profiles obtained by modeling are compared with the experiments. As it can be seen, the model accurately reproduces the pressure trend during the whole closed-cycle in both operating conditions. These results are in line with those reported in [38].

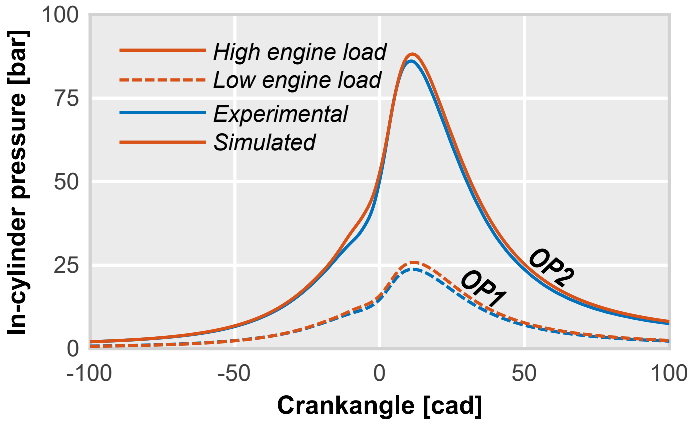

Figure 3: *Comparison of experimental and simulated in-cylinder pressure profiles for both operating engine loads.*

Besides this qualitative validation, additional parameters related to combustion were compared in Table 6. Both combustion parameters, CA50 and CA10-90, are also show a good agreement between experiments and simulations. Finally, due to the relevance of the engine efficiency as an indirect estimation of the emitted CO_2, the indicated efficiency gross is also included in the analysis. Again, results are encouraging since the gap among simulations and experiments is around 0.2% in both operating conditions. Therefore, these results confirm the suitability of the model for performing further studies.

Table 6: *Validation of combustion related parameters.*

		Experiment	**Model**
	CA50 [cad]	17.8	18.1
OP1	CA10-90 [cad]	35.4	34.7
	Indicated eff. gross [%]	35.9	36.1
	CA50 [cad]	5.4	5.2
OP2	CA10-90 [cad]	33.2	33.3
	Indicated eff. gross [%]	44.3	44.5

2.2.2. 1D jet model

A 1D in-house jet model [41, 42, 43, 44] used to estimate the hot jet characteristics during the pre-chamber ejection. The conservation equations are solved in terms of on-axis variables assuming self-similar radial profiles for the fuel mass fraction and velocity. The inputs of the model are the jet momentum flux and the mass flow rate at the nozzle exit, allowing to consider the instantaneous density inside the main chamber instead of a static value.

In this case, and due to the lack of an optical access in the engine, the jet model was validated by a computational fluid dynamics (CFD) model validated in [36, 45] over a wide range of operating conditions. The CFD model accounts for all local thermo-dynamic properties of the flow through a complete engine cycle, including the combustion-turbulence interaction. With this target in mind, the hot jet penetration can be estimated by both models by different processing methods. Results of this procedure can be found in Fig. 4, in which the instantaneous penetration of a single jet is shown. As it can be seen, the jet model provides comparable results in both operating conditions.

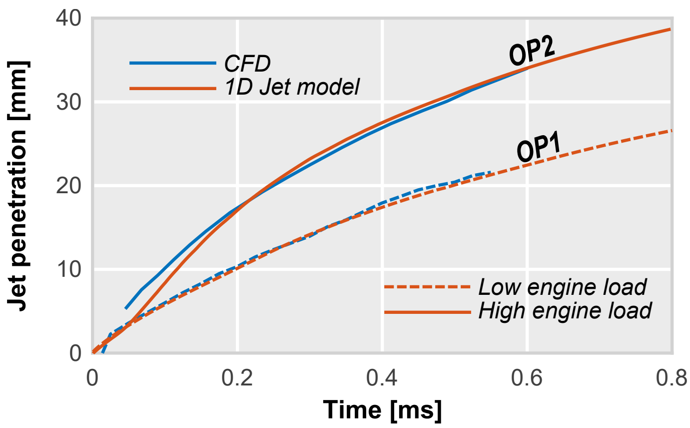

Figure 4: *Comparison of 1D jet and CFD models results. The jet penetration for two different operating points are contrasted.*

3. Results

3.1. Understanding the role of the jet momentum

Since jet momentum is directly related to the ability of the jet to advance from the discharge hole through the main combustion chamber and eventually initiating combustion in multiple locations, it can be considered as one of the key parameters to control the jet features.

The evolution of the ΔP among the high engine load and the low engine load cases is presented in Fig. 5, this pressure difference between pre and main chamber mostly drives the evolution of the jet momentum. The ΔP evolution can be divided into four different stages: filling, ejection, backflow re-filling and emptying. The first stage is dominated by the compression stroke, which forces the mixture to enter into the pre-chamber. The second stage corresponds to the ejection process, here, combustion starts inside the pre-chamber, and the consequent pressure increase forces the jets to enter into the main chamber. During the third stage, combustion occurs in the main chamber, increasing the pressure and forcing again a pre-chamber filling however, during this period, the pre-chamber is mostly filled by residual gases. Finally, the exhaust stroke dominates the fourth stage, emptying the pre-chamber.

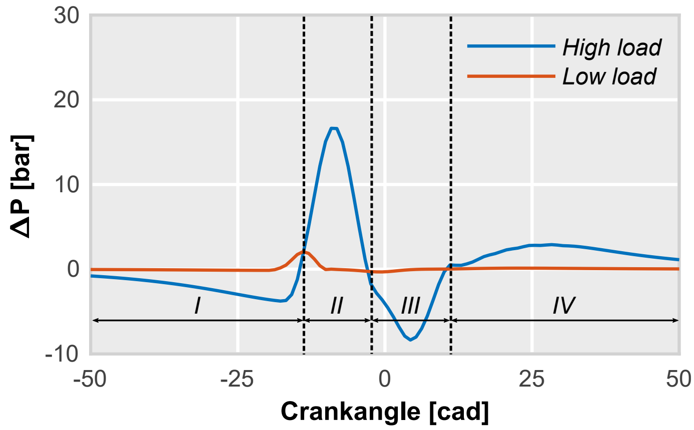

Figure 5: *Profile of ΔP between pre and main chambers for the high engine load case and the low engine load case.*

Results of the jet momentum profiles for the high and low load cases, including the fuel mass available in the pre-chamber at the start of combustion, are shown in Fig. 6. As it can be seen, jet momentum is strongly affected by the available fuel mass inside the pre-chamber at the start of combustion. The high load case profile is clearly higher than the low load case, being up to 7 times higher at the ejection peak (2^{nd} stage).

These results confirm that an increment of the fuel mass inside the pre-chamber will turn into higher jet momentum and a better sweeping of the main chamber. Following with the this hypothesis, one solution to increase this parameter is directly modifying the pre-chamber volume.

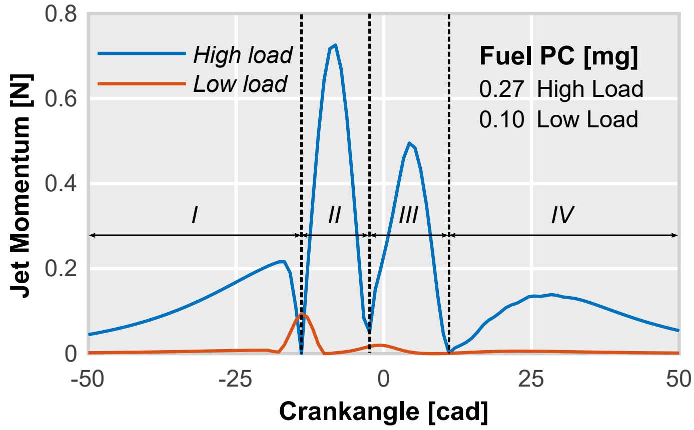

Figure 6: *Profile of the jet momentum for the high load case and the low load case and mass fuel available inside the pre-chamber at start of ejection.*

In this way, a study with the 1D wave action model has been carried out to evaluate the impact of the PC volume and the total holes area. The start of combustion and combustion duration of the pre-chamber have been fixed at the reference values (start at -16 cad ATDC and duration 12 cad), while the total hole cross sectional area and the pre-chamber volume were swept from 0.75 mm^2 to 12.0 mm^2, and from 400 mm^3 to 1000 mm^3, respectively. Figure 7 summarizes the outcomes of this study, showing the results of the maximum jet momentum peak as these two parameters are changed.

A clear trend towards increasing the maximum jet momentum peak when modifying the pre-chamber volume is observed if the holes cross sectional area is kept constant. This is mainly caused by the increased fuel mass at the start of pre-chamber combustion (fuel mass for the reference volume is 0.10 mg, while for a 950 mm^3 volume is 0.17 mg). As the fuel mass is higher, the total energy available to transfer to the jets increases, moving the jet momentum value peak towards higher levels (there is an increase from 0.068 N to 0.104 N). Regarding the cross sectional area, an optimum value can be found if the pre-chamber volume is fixed. For a small volume, the pressure drop is high and the amount of fuel within the pre-chamber is compromised. On the contrary, if the volume of the pre-chamber is too large, combustion is not able to progress quickly enough to increase the pre-chamber pressure, affecting the ejection process negatively.

Furthermore, the effect of the operating condition on the jet momentum was also studied. In Fig. 8, the effect of the variation of pre-chamber volume and total hole cross sectional area is presented for the high load condition (OP2). In this study, the pre-chamber combustion parameters and pre-chamber

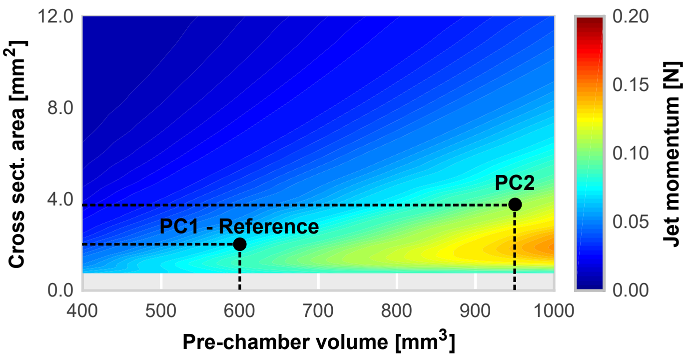

Figure 7: *Maximum jet momentum peak map for PC1 at low engine load conditions (OP1), considering the same pre-chamber combustion characteristics (starting and duration timings).*

geometric parameters are the same as those of low engine load study to isolate the effects of the engine load. Results show similar trends as for the low engine load case. However, the maximum jet momentum peak values are around ten times higher compared to low load levels. Therefore, the geometric requirements for a given pre-chamber are less restrictive at high loads than at low loads.

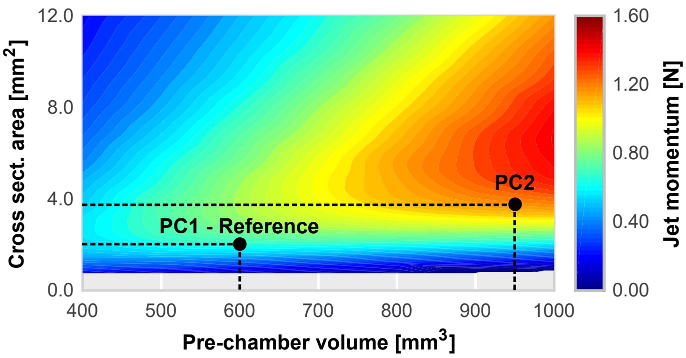

Figure 8: *Maximum jet momentum peak map for PC1 at high engine load conditions (OP2), considering the same pre-chamber combustion characteristics (starting and duration timings)*

In view of these results, a new pre-chamber geometry was selected (PC2), being a compromise solution in between of the two operating conditions. This new pre-chamber is intended to increase the jets surface for igniting the main chamber in both loads, which will turn into a better combustion process and a greater performance.

Since the 1D wave action model does not include a predictive combustion model, an additional modeling study was performed to quantify the impact of the combustion law inside the pre-chamber. In this way, the pre-chamber combustion onset was varied between (-20 cad aTDC and -10 cad aTDC), while the combustion duration was modified between 8 cad and 20 cad, being representative ranges of the real engine operation. In this study, the pre-chamber volume and the cross sectional area of the holes were kept constant to the PC1 reference values to isolate the effect of the combustion.

Figure 9 presents the results of this numerical study, showing two clear trends. Regarding the combustion duration, the maximum ΔP between the chambers and, subsequently, the maximum jet momentum increase as combustion rates increase. These results confirm how the most favorable situation for the pre-chamber ignition concept is established by an instantaneous combustion. The onset of combustion shows a similar trend. Since the amount of fuel inside the pre-chamber increases as combustion is delayed towards TDC due to extra-filling caused by the piston compression, the maximum jet momentum peak significantly increases; the effect is similar than that of increasing the pre-chamber volume.

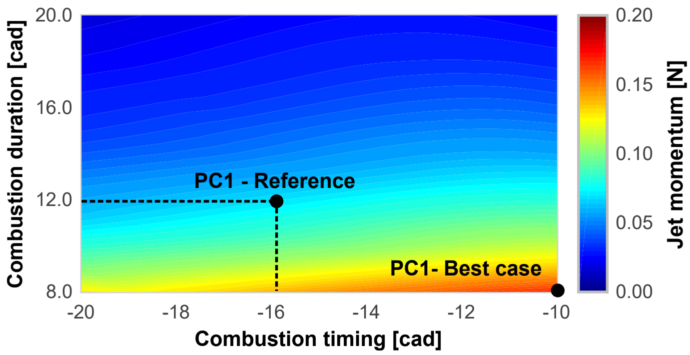

Figure 9: *Maximum jet momentum peak map for PC1 for reference and best case at low engine load conditions (OP1), considering the same the pre-chamber volume and the total holes area.*

To clearly identify the benefits of a higher pre-chamber energy release, Fig. 10 shows the heat release rate in the pre-chamber and the resulting jet momentum for both, the PC1 reference combustion and the best PC1 combustion. It is shown how a faster combustion turns into a sharper jet momentum profile that improves the overall performance of jets.

3.2. The effect of the jet momentum on jet penetration

The next step in the investigation was to understand how the jet momentum profile affects the jet penetration. Therefore, a study which combines both 1D models was carried out. As described in previous sections, the 1D jet model estimates the transient penetration of a free jet using the diameter

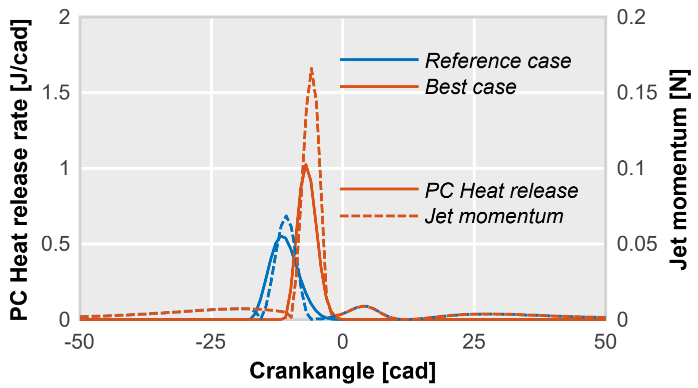

Figure 10: *Rate of heat release and jet momentum flux of PC1 for both reference and best case at low engine load conditions (OP1), considering the same the pre-chamber volume and the total holes area.*

of the nozzle hole, the effective ejection velocity profile (obtained from the momentum and the mass flow rate profiles) and the donwstream thermodynamic conditions in the main combustion chamber. From this outcome, the model calculates the time it takes for the jet to reach the cylinder wall (t*).

The jet penetrations generated by PC1 and PC2 are plotted in Fig. 11. The distance to the farthest cylinder wall is included with a black dashed line for reference. It can be seen how increasing the jet momentum (PC2) results in a faster jet penetration. This fact reduces the time needed to reach the cylinder walls, producing larger reaction surfaces for igniting the main chamber in less time. Therefore, this parameter (t*) is a clear indicator of the performance of the pre-chamber, being a suitable benchmark for characterizing its operation.

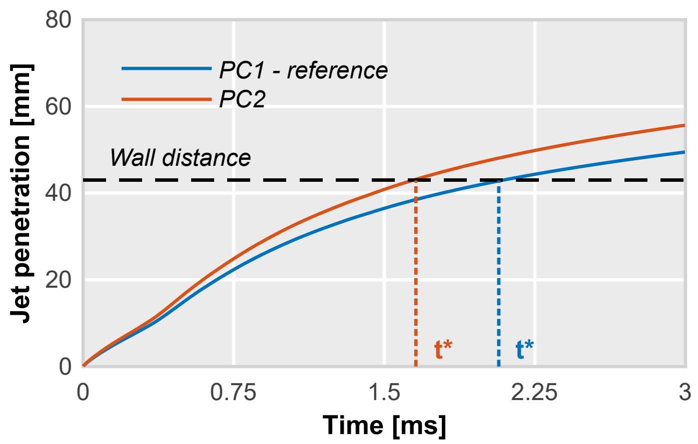

Figure 11: *Map of t* for PC1 at high engine load conditions, considering the same pre-chamber combustion characteristics (starting and duration timings).*

In Fig. 12, results of the full study are presented for the low engine load case (OP1). The pre-chamber volume and the hole cross sectional area were swept between the same ranges used in the previous section: pre-chamber volume varies from 400 to 1000 mm^3 and hole cross sectional from 0.75 to 12.0 mm^2).

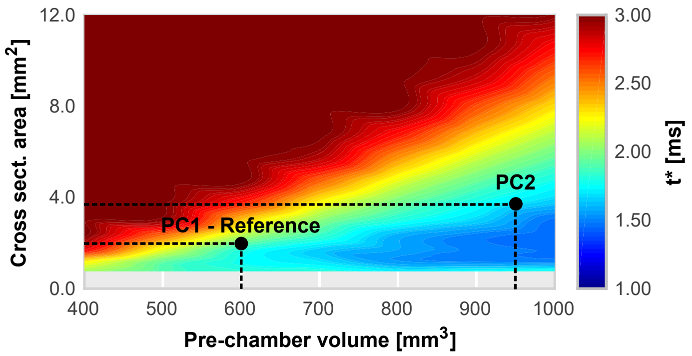

Figure 12: *Map of t* for PC1 at low engine load conditions (OP1), considering the same pre-chamber combustion characteristics (starting and duration timings).*

As results show, both maps analyzed so far, the maximum jet momentum peak and the t*, are some how related to each other. This fact gives consistency to the numerical methodology and it highlights coherence among both models. The bigger the pre-chamber volume, the higher the jet momentum peak and the lower the time to reach the cylinder wall. Again, the new pre-chamber (PC2) is in a more favorable region compared to the original (PC1) pre-chamber. However, these conclusions are only valid if the combustion process inside the pre-chamber is similar in any of the pre-chamber definitions. As showed in the previous study, the resulting t* will change accordingly, if the combustion process is remarkably different.

The same analysis was performed at the high engine load conditions. Results of this study are presented in Fig. 13. It is important to highlight that the t* values are clearly decreased (from 1.5 ms to 0.5 ms approx.), making larger the optimum area compared to the low engine load case. However, although increasing the pre-chamber volume has positive results in both operating conditions, the impact of the holes area is different. While the optimum region for a 1000 mm^3 PC is around 2 mm^2 at low engine load, it increases up to 6 mm^2 at high engine loads.

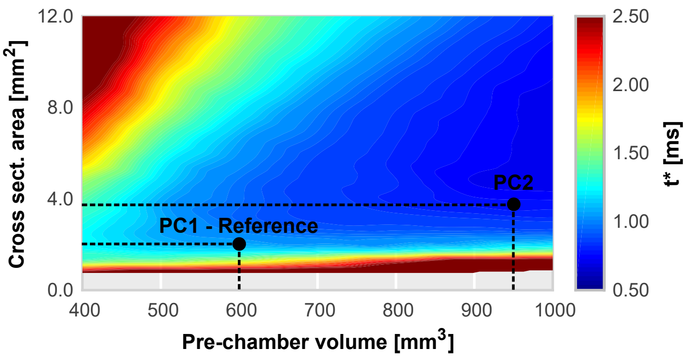

Figure 13: *Map of t* for PC1 at high engine load conditions (OP2), considering the same pre-chamber combustion characteristics (starting and duration timings).*

3.3. Experimental evaluation of pre-chambers

Experimental activities related to the final validation of the methodology are divided into two main studies. In the first one, the proposed pre-chamber design (PC2) was manufactured and experimentally tested on the engine to evaluate impact of increasing the pre-chamber volume while keeping a suitable total hole area. The second study is focused on further analyzing the effect of the pre-chamber geometry on the concept performance. In particular, the impact of an additional geometric parameter, the nozzles orientation or indirectly the internal swirl level of the PC, is studied. In both studies, the two operating conditions considered so far are considered. Besides, the spark timing was swept using the OP1 and the effect of EGR dilution was analyzed using OP2.

3.3.1. Impact of the pre-chamber geometry

The main specifications of pre-chambers studied in this section are presented in Table 7. The spark timing sweep was made in steps of 2 cad for the pre-chambers and 4 cad for the spark ignition, full details about these experimental activities can be found in Table 2.

Figure 14 compares some relevant engine outputs against the spark timing for the three ignition systems (note that the conventional SI system is included for reference) operating at low engine load and speed (OP1).

As it can be seen, the maximum rate of heat release (HRR) is increased when considering a larger pre-chamber volume (PC2). This increase in the combustion velocity also coincides on an enhanced combustion phasing (CA50). As the burning rate for the smaller pre-chamber (PC1) is lower, the combustion phasing is moved towards the expansion stroke, far from both the conventional spark system

Table 7: Main specifications of PC1 and PC2.

	Pre-chamber 1 (PC1)	Pre-chamber 2 (PC2)
Volume [mm^3]	600	950
Hole area [mm^2]	2.3	3.8
Number of holes [-]	6	6

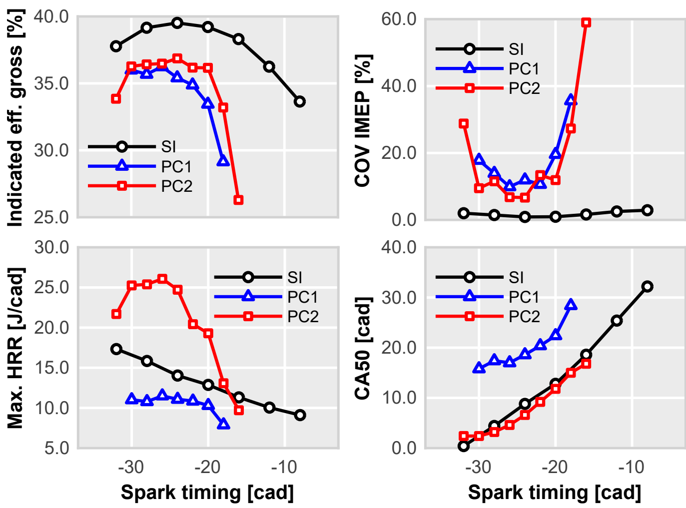

Figure 14: Trends of gross indicated efficiency, combustion stability, maximum heat release rate and combustion phasing for the pre-chamber geometry study at low engine load and speed conditions (OP1).

(SI) and the PC2. Due to these facts, PC2 exhibit higher levels of gross indicated efficiency in the whole operating range. However, these efficiency levels are still far from those obtained by the conventional SI system. The observed trends validate again the numerical methodology, since the increment of available energy inside the pre-chamber helps to improve the overall performance of the concept.

Regarding the combustion stability, quantified by the covariance of the IMEP, both pre-chambers are more unstable than conventional SI system. In general, the pre-chambers COV IMEP is higher through the whole spark timing sweep whereas effective operating range is notably reduced (10 cad for both PCs and almost complete flexibility for conventional SI).

The next step in the experimental activities was to evaluate the tolerance to external EGR dilution at high engine speeds and loads. In this case, the EGR level was swept in steps of 5% until the combustion stability was extremely compromised (reaching covariance values over 20%). As in the previous figure, the gross indicated efficiency, combustion stability, maximum heat release rate and combustion phasing against the EGR dilution rate are shown in Fig. 15.

Results show that larger pre-chamber volumes are able to slightly extend the maximum dilution limit. Note that the drop observed in the gross indicated efficiency occurs at a higher dilution levels for PC2. The levels of maximum HRR are higher for PC2, even at high dilution ratios. The combustion phasing oscillates between 5 and 10 CAD aTDC when combustion stability is maintained at acceptable values (well below 5% of COV IMEP). The increase of this instability affects the gross indicated efficiency, as observed in the previous operating point (OP1). Nevertheless, the efficiency levels are similar or slightly better for both pre-chambers when combustion stability is maintained.

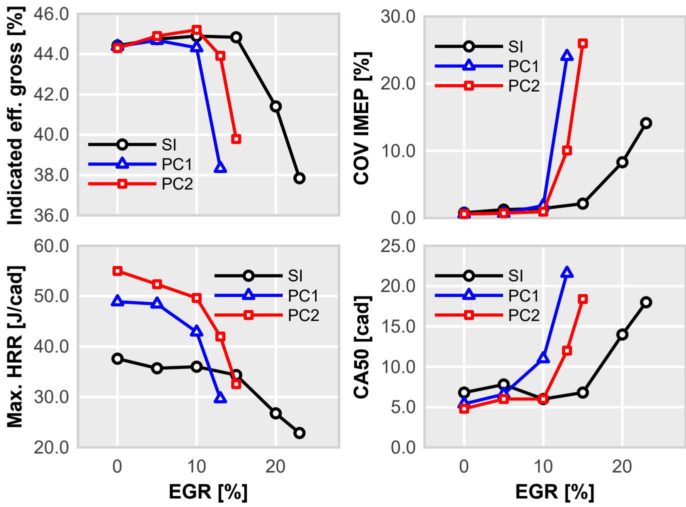

Figure 15: *Trends of gross indicated efficiency, combustion stability, maximum heat release rate and combustion phasing as the EGR level is modified at high engine load and speed conditions (OP2).*

3.3.2. Impact of the nozzles orientation

The effect of the holes orientation was experimentally evaluated due to the models limitation. A new set of pre-chambers were manufactured with different tangential angles. Their specifications are shown in Table 8. Again, the same methodology described in Table 2, and followed in the previous sections, is used here for sweeping both the spark timing and the EGR dilution level.

Table 8: Main specifications of the new set of pre-chambers.

	Pre-chamber 1		
	(PC1)	(PC1b)	(PC1c)
Volume [mm^3]	600	600	600
Hole diameter [mm]	0.7	0.7	0.7
Number of holes [-]	6	6	6
Nozzles tangential angle [degrees]	7.5	12.5	0

In Fig. 16 experimental results of this study operating at OP1 are presented following the same representation used in the previous studies.

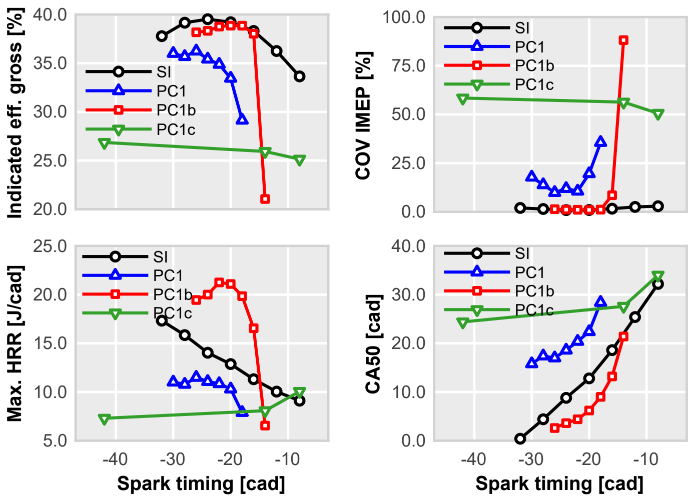

Figure 16: *Effect of the nozzles orientation in terms of gross indicated efficiency, combustion stability, maximum heat release rate and combustion phasing as the spark timing is modified at low engine load and speed conditions (OP1).*

As this figure shows, there are three different levels of combustion stability that corresponds with the three levels of tangential angles. The pre-chamber performance is scaled with their respective combustion stability. When increasing the tangential angle of the pre-chamber nozzles, the swirl level inside the pre-chamber increases, stabilizing the combustion process. The combustion phasing and the burning rate are also related to the combustion stability. While the maximum combustion velocity increases with a more stable design, its combustion phasing is moved towards TDC.

The PC1b definition is the most stable among all pre-chambers, whereas PC1c has only three measured points due to the extremely high variability experienced during experiments. Indeed, PC1b operates at same level as the conventional SI, at least until the characteristic drop of combustion stability appears in the pre-chamber case. The extremely high dispersion shown by PC1c strongly conditioned the results, however, it seems that the combustion phasing is excessively shifted towards the expansion stroke.

Next, the performance of this new set of pre-chambers were evaluated under EGR diluted conditions when operating at high engine load and speed (OP2). Results of experiments are presented in Fig. 17.

In this case, the reference pre-chamber (PC1) shows the maximum dilution limit, while the two new pre-chambers are not able to operate at the same dilution level with comparable stability levels. The indicated efficiency of this pre-chamber is higher than the other two, being the improved combustion speed and phasing the main reasons. Therefore, while increasing the swirl level helps to stabilize combustion at non diluted conditions, the tolerance to external EGR is established by an optimum value.

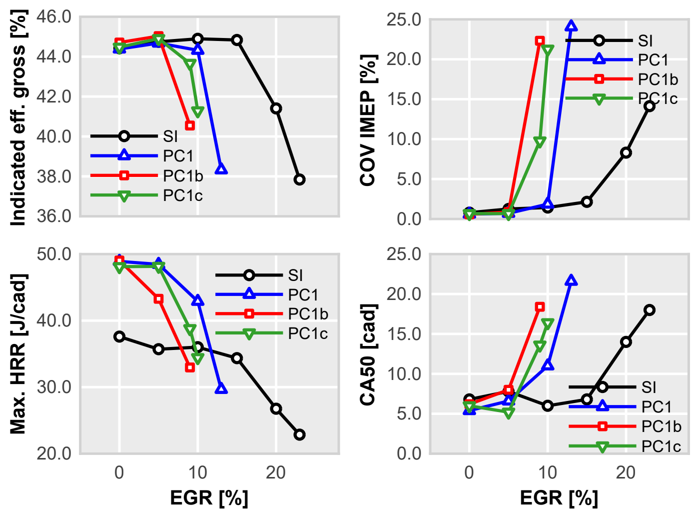

Figure 17: *Effect of the nozzles orientation in terms of gross indicated efficiency, combustion stability, maximum heat release rate and combustion phasing as the EGR level is modified at high engine load and speed conditions (OP2).*

4. Discussion

Numerical results showed how large pre-cambers boost the maximum jet momentum as long as the total area of the holes is compatible with the pre-chamber volume. In addition, while a faster combustion results in a higher jet momentum flux, phasing the PC combustion close the TDC helps to increase the energy available for igniting the main chamber. In this sense, a faster combustion inside the pre-chamber favors the overall performance of the concept, as it has been also proven by Attard et al. [15, 46] and Shah et al. [25].

Moreover, the jet penetration depends on the ability of the pre-chamber to transfer this energy to the jets. A higher jet momentum will turn into a deeper jet penetration into the main chamber, reducing the time to reach the cylinder walls while increasing the reacting surface for igniting it. These results agree with the work performed by Thelen et al. [47]. However, results shown that a well-designed pre-chamber working optimally at a given specific condition will not operate properly in another one. This confirms that the geometric pre-chamber requirements are strongly related to the operating condition, making difficult to find an optimum design for the whole engine map.

Experimental activities confirmed that, larger pre-chamber volumes help to increase the operating range at low engine load and speed conditions and increase the maximum EGR dilution level at high engine load and speed conditions. However, results also show that it is mandatory to improve the combustion stability for achieving further levels of tolerance to external EGR. Similar conclusions regarding the combustion stability when increasing dilution are provided in the literature by Vedula et al. [48], Slefarski et al. [49] or Jamrozik et al. [32] among many others. The efficiency gap between both combustion systems is a consequence of the increased heat loss due to the combustion shortening and the combustion stability worsening [36].

The efficiency results reported in Figs. 14 and 16, suggest that a proper combination of pre-chamber size and tangential angle of the nozzle holes could be the right path for the concept optimization, allowing significant improvements of combustion stability at low load and speed conditions. In addition, such combination does not have to be an advantage in terms of external EGR tolerance. As shown in Figs.15 and 17, there is no clear relationship between the internal pre-chamber swirl level and the maximum EGR dilution limit. Since the maximum EGR tolerance depends on the pre-chamber scavenge and filling processes, the residuals stratification inside the pre-chamber should play a relevant role in the combustion process. Thus, an increased swirl level can negatively affect to the internal pre-chamber scavenge modifying the effective EGR dilution level close to the spark plug electrodes [45]. This represents a important issue in the current pre-chamber configurations since the spark plug is located at the top of the pre-chamber body where most of the residual gas is accumulated. Nevertheless, there exists an optimum angle that maximizes the EGR tolerance, leading to a slight improvement in combustion stability while keeping competitive efficiency levels. However, this improvement will not be enough to reach the dilution limit achieved by the conventional spark ignition system.

In light of these results, the passive pre-chamber ignition system can not be completely optimized by only considering the three geometrical parameters used in this investigation. Thus, new technological solutions, such as advanced internal geometries and/or improved igniter features, should be explored and deeply evaluated.

An alternative to the rigidity of the passive pre-chamber, the active concept, with a dedicated fuel supply system inside the pre-chamber, is probably more adaptive to optimize the concept in the whole engine map. This concept not only allows to control the reactivity of the pre-chamber charge independently of the main chamber, but also helps to sweep the residual gas and to stratify the mixture in the region of spark electrodes, with the surrounding leaner mixture.

5. Summary and conclusions

The passive pre-chamber ignition concept has been numerically and experimentally evaluated at two different operating condition points in a turbo-charged high-compression ratio Miller-cycle engine. Results focused on identifying relationships between the pre-chamber design and its impact on the engine efficiency, contributing to optimizing the concept in its broadest sense.

The numerical methodology that combines 1D wave action and 1D jet modeling has proven to be a valuable tool to analyze the performance of the jets while reducing computing costs. In addition, a key parameter, named t*, that allow comparing different pre-chamber definitions at distinct operating points has been proposed.

Results of these simulations show that larger pre-chamber volumes increase the performance of the jets as long as the total hole area is properly set. Since the energy available inside the pre-chamber at the start of combustion is higher due to the increased pre-chamber volume, the performance of the concept increases at both operating conditions studied. It has been also proven that increasing the maximum rate of heat release in the pre-chamber will result into a higher jet momentum flux even if the fuel mass inside the PC is kept constant.

The system requirements strongly depends on the operating condition. Therefore, there is not a proper combination of pre-chamber volume and holes area that optimizes the performance of the concept in the whole operation map. In this way, the target operation is a critical aspect in the design process and it is strongly reliant on the specific application (conventional ICE application, range-extender, etc.).

Experimental results confirmed the trends observed in the simulations, thus validating the numerical methodology for the pre-chamber design. Indeed, the proposed pre-camber definition increases the gross indicated efficiency in the whole studied range.

Results also showed that the combustion stability is scaled with the internal swirl level of the pre-chamber. When tangential angle is increased the combustion instability is notably reduced, achieving similar levels than those observed in the conventional spark ignition system. On the contrary, the combustion stability is extremely compromised when considering completely radial holes with no tangential angle.

Finally, a trade-off trend between the pre-chamber swirl level and the external EGR tolerance has been identified. Although an increased swirl level helps to stabilize combustion, it affects negatively the pre-chamber scavenge, resulting in a lower EGR tolerance.

Acknowledgements

The work has been partially supported by the Spanish Ministerio de Economía y Competitividad through grant number TRA2017-89139-C2-1-R.

P. J. Martinez-Hernandiz is partially supported by an FPI contract (FPI-S2-19-21993) of the “Programa de Apoyo para la Investigación y Desarrollo (PAID-05-19)” of the Universitat Politècnica de València.

The authors also wish to thank Mr. Gabriel Alcantarilla for his inestimable assistance during the experimental campaign.

References

[1] S. J. Davis, K. Caldeira, Consumption-based accounting of co2 emissions, Proceedings of the National Academy of Sciences 107 (12) (2010) 5687–5692.

[2] A. Malik, J. Lan, M. Lenzen, Trends in global greenhouse gas emissions from 1990 to 2010, Environmental science & technology 50 (9) (2016) 4722–4730.

[3] J. Burck, F. Marten, C. Bals, N. Höhne, The climate change performance index: Results 2014, Germanwatch Berlin, 2014.

[4] J. Lelieveld, J. S. Evans, M. Fnais, D. Giannadaki, A. Pozzer, The contribution of outdoor air pollution sources to premature mortality on a global scale, Nature 525 (7569) (2015) 367.

[5] F. A. Ayala, M. D. Gerty, J. B. Heywood, Effects of combustion phasing, relative air-fuel ratio, compression ratio, and load on si engine efficiency, in: SAE 2006 World Congress & Exhibition, SAE International, 2006. doi:https://doi.org/10.4271/2006-01-0229.
URL https://doi.org/10.4271/2006-01-0229

[6] A. Königstein, U. D. Grebe, K.-J. Wu, P.-I. Larsson, Differentiated analysis of downsizing concepts, MTZ worldwide 69 (6) (2008) 4–11. doi:10.1007/BF03227890.
URL https://doi.org/10.1007/BF03227890

[7] P. Leduc, B. Dubar, A. Ranini, G. Monnier, Downsizing of gasoline engine: an efficient way to reduce co2 emissions, Oil & Gas Science and Technology - Rev. IFP 58 (1) (2003) 115–127. doi:10.2516/ogst:2003008.
URL https://doi.org/10.2516/ogst:2003008

[8] G. J. Germane, C. G. Wood, C. C. Hess, Lean combustion in spark-ignited internal combustion engines - a review, in: 1983 SAE International Fall Fuels and Lubricants Meeting and Exhibition, SAE International, 1983. doi:https://doi.org/10.4271/831694.
URL https://doi.org/10.4271/831694

[9] F. A. Ayala, J. B. Heywood, Lean si engines: The role of combustion variability in defining lean limits, in: 8th International Conference on Engines for Automobiles, Consiglio Nazionale delle Ricerche, 2007. doi:https://doi.org/10.4271/2007-24-0030.
URL https://doi.org/10.4271/2007-24-0030

[10] Y. long Bai, Z. Wang, J. xin Wang, Part-load characteristics of direct injection spark ignition engine using exhaust gas trap, Applied Energy 87 (8) (2010) 2640 – 2646. doi:https://doi.org/10.1016/j.apenergy.2010.03.012.
URL http://www.sciencedirect.com/science/article/pii/S0306261910000760

[11] W. P. Attard, H. Blaxill, A lean burn gasoline fueled pre-chamber jet ignition combustion system achieving high efficiency and low nox at part load, in: SAE 2012 World Congress & Exhibition, SAE International, 2012. doi:https://doi.org/10.4271/2012-01-1146.
URL https://doi.org/10.4271/2012-01-1146

[12] J. Dale, M. Checkel, P. Smy, Application of high energy ignition systems to engines, Progress in Energy and Combustion Science 23 (5) (1997) 379 – 398. doi:https://doi.org/10.1016/S0360-1285(97)00011-7.
URL http://www.sciencedirect.com/science/article/pii/S0360128597000117

[13] S. Schlatter, B. Schneider, Y. M. Wright, K. Boulouchos, Comparative study of ignition systems for lean burn gas engines in an optically accessible rapid compression expansion machine, in: 11th International Conference on Engines & Vehicles, SAE International, 2013. doi:https://doi.org/10.4271/2013-24-0112.
URL https://doi.org/10.4271/2013-24-0112

[14] T. Briggs, T. Alger, B. Mangold, Advanced ignition systems evaluations for high-dilution si engines, SAE International Journal of Engines 7 (4) (2014) 1802–1807. doi:https://doi.org/10.4271/2014-01-2625.
URL http://www.jstor.org/stable/26277889

[15] W. P. Attard, M. Bassett, P. Parsons, H. Blaxill, A new combustion system achieving high drive cycle fuel economy improvements in a modern vehicle powertrain, in: SAE 2011 World Congress & Exhibition, SAE International, 2011. doi:https://doi.org/10.4271/2011-01-0664.
URL https://doi.org/10.4271/2011-01-0664

[16] W. P. Attard, H. Blaxill, A gasoline fueled pre-chamber jet ignition combustion system at unthrottled conditions, SAE International Journal of Engines 5 (2) (2012) 315–329. doi:https://doi.org/10.4271/2012-01-0386.
URL https://doi.org/10.4271/2012-01-0386

[17] W. P. Attard, P. Parsons, A normally aspirated spark initiated combustion system capable of high load, high efficiency and near zero nox emissions in a modern vehicle powertrain, SAE International Journal of Engines 3 (2) (2010) 269–287. doi:https://doi.org/10.4271/2010-01-2196.
URL https://doi.org/10.4271/2010-01-2196

[18] W. P. Attard, J. Kohn, P. Parsons, Ignition energy development for a spark initiated combustion system capable of high load, high efficiency and near zero nox emissions, SAE International Journal of Engines 3 (2) (2010) 481–496. doi:https://doi.org/10.4271/2010-32-0088.
URL https://doi.org/10.4271/2010-32-0088

[19] W. P. Attard, P. Parsons, Flame kernel development for a spark initiated pre-chamber combustion system capable of high load, high efficiency and near zero nox emissions, SAE International Journal of Engines 3 (2) (2010) 408–427. doi:https://doi.org/10.4271/2010-01-2260.
URL https://doi.org/10.4271/2010-01-2260

[20] G. Gentz, B. Thelen, P. Litke, J. Hoke, E. Toulson, Combustion visualization, performance, and cfd modeling of a pre-chamber turbulent jet ignition system in a rapid compression machine, SAE International Journal of Engines 8 (2) (2015) 538–546. doi:https://doi.org/10.4271/2015-01-0779.
URL https://doi.org/10.4271/2015-01-0779

[21] G. Gentz, M. Gholamisheeri, E. Toulson, A study of a turbulent jet ignition system fueled with iso-octane: Pressure trace analysis and combustion visualization, Applied Energy 189 (2017) 385 – 394. doi:https://doi.org/10.1016/j.apenergy.2016.12.055.
URL http://www.sciencedirect.com/science/article/pii/S0306261916318189

[22] S. Biswas, S. Tanvir, H. Wang, L. Qiao, On ignition mechanisms of premixed ch4/air and h2/air using a hot turbulent jet generated by pre-chamber combustion, Applied Thermal Engineering 106 (2016) 925 – 937. doi:https://doi.org/10.1016/j.applthermaleng.2016.06.070.
URL http://www.sciencedirect.com/science/article/pii/S135943111630984X

[23] S. Biswas, L. Qiao, Ignition of ultra-lean premixed h2/air using multiple hot turbulent jets generated by pre-chamber combustion, Applied Thermal Engineering 132 (2018) 102 – 114. doi:https://doi.org/10.1016/j.applthermaleng.2017.11.073.
URL http://www.sciencedirect.com/science/article/pii/S1359431117353000

[24] S. Biswas, L. Qiao, Ignition of ultra-lean premixed hydrogen/air by an impinging hot jet, Applied energy 228 (2018) 954–964.

[25] A. Shah, P. Tunestal, B. Johansson, Effect of pre-chamber volume and nozzle diameter on pre-chamber ignition in heavy duty natural gas engines, in: SAE 2015 World Congress & Exhibition, SAE International, 2015. doi:https://doi.org/10.4271/2015-01-0867.
URL https://doi.org/10.4271/2015-01-0867

[26] B. C. Thelen, E. Toulson, A computational study on the effect of the orifice size on the performance of a turbulent jet ignition system, Proceedings of the Institution of Mechanical Engineers, Part D: Journal of Automobile Engineering 231 (4) (2017) 536–554.

[27] P. Allison, M. de Oliveira, A. Giusti, E. Mastorakos, Pre-chamber ignition mechanism: Experiments and simulations on turbulent jet flame structure, Fuel 230 (2018) 274 – 281. doi:https://doi.org/10.1016/j.fuel.2018.05.005.
URL http://www.sciencedirect.com/science/article/pii/S0016236118308287

[28] M. Bunce, H. Blaxill, Methodology for combustion analysis of a spark ignition engine incorporating a pre-chamber combustor, in: SAE 2014 International Powertrain, Fuels & Lubricants Meeting, SAE International, 2014. doi:https://doi.org/10.4271/2014-01-2603.
URL https://doi.org/10.4271/2014-01-2603

[29] E. Mastorakos, P. Allison, A. Giusti, P. De Oliveira, S. Benekos, Y. Wright, C. Frouzakis, K. Boulouchos, Fundamental aspects of jet ignition for natural gas engines, JSTOR, 2017. doi:https://doi.org/10.4271/2017-24-0097.
URL https://doi.org/10.4271/2017-24-0097

[30] A. Shah, P. Tunestal, B. Johansson, Effect of relative mixture strength on performance of divided chamber 'avalanche activated combustion' ignition technique in a heavy duty natural gas engine, in: SAE 2014 World Congress & Exhibition, SAE International, 2014. doi:https://doi.org/10.4271/2014-01-1327.
URL https://doi.org/10.4271/2014-01-1327

[31] S. Heyne, M. Meier, B. Imbert, D. Favrat, Experimental investigation of prechamber autoignition in a natural gas engine for cogeneration, Fuel 88 (3) (2009) 547 – 552. doi:https://doi.org/10.1016/j.fuel.2008.09.032.
URL http://www.sciencedirect.com/science/article/pii/S0016236108003712

[32] A. Jamrozik, Lean combustion by a pre-chamber charge stratification in a stationary spark ignited engine, Journal of Mechanical Science and Technology 29 (5) (2015) 2269–2278. doi:https://doi.org/10.1007/s12206-015-0145-7.

[33] J. Benajes, R. Novella, J. Gomez-Soriano, P. Martinez-Hernandiz, C. Libert, M. Dabiri, Performance of the passive pre-chamber ignition concept in a spark-ignition engine for passenger car applications, in: SIA Powertrain & Electronics, 2019.

[34] M. Sens, E. Binder, Pre-chamber ignition as a key technology for future powertrain fleets, MTZ worldwide 80 (2) (2019) 44–51. doi:10.1007/s38313-018-0150-1.
URL https://doi.org/10.1007/s38313-018-0150-1

[35] M. Kettner, M. Rothe, A. Velji, U. Spicher, D. Kuhnert, R. Latsch, A new flame jet concept to improve the inflammation of lean burn mixtures in si engines, SAE transactions (2005) 1549–1557.

[36] J. Benajes, R. Novella, J. Gomez-Soriano, I. Barbery, C. Libert, F. Rampanarivo, M. Dabiri, Computational assessment towards understanding the energy conversion and combustion process of lean mixtures in passive pre-chamber ignited engines, Applied Thermal Engineering 178 (2020) 115501. doi:https://doi.org/10.1016/j.applthermaleng.2020.115501.
URL http://www.sciencedirect.com/science/article/pii/S1359431120329835

[37] C. Müller, B. Morcinkowski, C. Schernus, K. Habermann, T. Uhlmann, Development of a pre-chamber for spark ignition engines in vehicle applications (2018).

[38] J. Benajes, R. Novella, J. Gomez-Soriano, P. Martinez-Hernandiz, C. Libert, M. Dabiri, Evaluation of the passive pre-chamber ignition concept for future high compression ratio turbocharged spark-ignition engines, Applied Energy 248 (2019) 576 – 588. doi:https://doi.org/10.1016/j.apenergy.2019.04.131.
URL http://www.sciencedirect.com/science/article/pii/S030626191930769X

[39] M. Lapuerta, O. Armas, J. Hernández, Diagnosis of di diesel combustion from in-cylinder pressure signal by estimation of mean thermodynamic properties of the gas, Applied Thermal Engineering 19 (5) (1999) 513 – 529. doi:https://doi.org/10.1016/S1359-4311(98)00075-1.
URL http://www.sciencedirect.com/science/article/pii/S1359431198000751

[40] F. Payri, S. Molina, J. Martín, O. Armas, Influence of measurement errors and estimated parameters on combustion diagnosis, Applied Thermal Engineering 26 (2) (2006) 226 – 236. doi:https://doi.org/10.1016/j.applthermaleng.2005.05.006.
URL http://www.sciencedirect.com/science/article/pii/S1359431105001560

[41] J. V. Pastor, J. J. López, J. M. García, J. M. Pastor, A 1d model for the description of mixing-controlled inert diesel sprays, Fuel 87 (13) (2008) 2871 – 2885. doi:https://doi.org/10.1016/j.fuel.2008.04.017.
URL http://www.sciencedirect.com/science/article/pii/S0016236108001580

[42] J. Desantes, J. Pastor, J. García-Oliver, J. Pastor, A 1d model for the description of mixing-controlled reacting diesel sprays, Combustion and Flame 156 (1) (2009) 234 – 249. doi:https://doi.org/10.1016/j.combustflame.2008.10.008.
URL http://www.sciencedirect.com/science/article/pii/S0010218008003088

[43] J. Desantes, J. García-Oliver, T. Xuan, W. Vera-Tudela, A study on tip penetration velocity and radial expansion of reacting diesel sprays with different fuels, Fuel 207 (2017) 323 – 335. doi:https://doi.org/10.1016/j.fuel.2017.06.108.
URL http://www.sciencedirect.com/science/article/pii/S0016236117308177

[44] J. V. Pastor, J. M. Garcia-Oliver, J. M. Pastor, W. Vera-Tudela, One-dimensional diesel spray modeling of multicomponent fuels, Atomization and Sprays 25 (6) (2015) 485–517.

[45] R. Novella, J. Pastor, J. Gomez-Soriano, I. Barbery, C. Libert, F. Rampanarivo, C. Panagiotis, M. Dabiri, Experimental and numerical analysis of passive pre-chamber ignition with egr and air dilution for future generation passenger car engines, Tech. rep., SAE Technical Paper (2020).

[46] W. P. Attard, N. Fraser, P. Parsons, E. Toulson, A turbulent jet ignition pre-chamber combustion system for large fuel economy improvements in a modern vehicle powertrain, SAE International Journal of Engines 3 (2) (2010) 20–37. doi:https://doi.org/10.4271/2010-01-1457.
URL https://doi.org/10.4271/2010-01-1457

[47] B. C. Thelen, E. Toulson, A computational study of the effects of spark location on the performance of a turbulent jet ignition system, in: SAE 2016 World Congress and Exhibition, SAE International, 2016. doi:https://doi.org/10.4271/2016-01-0608.
URL https://doi.org/10.4271/2016-01-0608

[48] R. T. Vedula, G. Gentz, T. Stuecken, E. Toulson, H. Schock, Lean burn combustion of iso-octane in a rapid compression machine using dual mode turbulent jet ignition system (mar 2018). doi:https://doi.org/10.4271/03-11-01-0007.

[49] R. Ślefarski, M. Gołębiewski, P. Czyżewski, P. Grzymisławski, J. Wawrzyniak, Analysis of combustion process in industrial gas engine with prechamber-based ignition system, Energies 11 (2) (2018). doi:https://doi.org/10.3390/en11020336.
URL https://www.mdpi.com/1996-1073/11/2/336

List of Figures

List of Tables